Transient Rayleigh–Bénard–Marangoni convection due to evaporation: a linear non-normal stability analysis

F. DOUMENC[1]†, T. BOECK[2], B. GUERRIER[1] AND M. ROSSI[3]

[1]UPMC Université Paris 06, Université Paris-Sud, CNRS, UMR 7608, Lab FAST, Bat 502, Campus Universitaire, Orsay F-91405, France

[2]Institut für Thermo- und Fluiddynamik, Technische Universität Ilmenau, Postfach 100565, 98684 Ilmenau, Germany

[3]UPMC Université Paris 06, CNRS, UMR 7190, IJLRA, 4 place Jussieu, Paris F-75005, France

The convective instability in a plane liquid layer with time-dependent temperature profile is investigated by means of a general method suitable for linear stability analysis of an unsteady basic flow. The method is based on a non-normal approach, and predicts the onset of instability, critical wavenumber and time. The method is applied to transient Rayleigh–Bénard–Marangoni convection due to cooling by evaporation. Numerical results as well as theoretical scalings for the critical parameters as function of the Biot number are presented for the limiting cases of purely buoyancy-driven and purely surface-tension-driven convection. Critical parameters from calculations are in good agreement with those from experiments on drying polymer solutions, where the surface cooling is induced by solvent evaporation.

1. Introduction

Thermally driven flows near liquid interfaces continue to be an active area of research since the first experimental studies by H. Bénard over 100 years ago. They are characterized by a multitude of interacting physical mechanisms and display a large variety of regular and complex flow patterns. Experimental and theoretical studies of such flows have stimulated and accompanied the development of the theory of pattern formation and nonlinear phenomena in general. Recent developments are summarized in a number of monographs and review papers (see e.g. Bodenschatz, Pesch & Ahlers 2000; Colinet, Legros & Velarde 2001; Nepomnyashchy, Simanovskii & Legros 2006).

The driving forces in these thermally driven flows are surface-tension gradients (Marangoni forces) and buoyancy forces, which originate from the temperature dependency of surface tension and density, respectively. Both mechanisms are classically studied in convection taking place within a finite layer subjected to a steady temperature difference: for the buoyancy-driven case, this is the celebrated Rayleigh–Bénard convection formulated by Rayleigh (1916), for the surface-tension-driven case this is the Bénard–Marangoni convection studied by Pearson (1958). In both

† Email address for correspondence: frederic.doumenc@upmc.fr

cases, a certain critical temperature difference must be applied in order to sustain convective motion. The theoretical predictions for such critical temperature differences are in excellent agreement with experiments (Chandrasekhar 1961; Schatz *et al.* 1995). Thermal convection can also appear when the external conditions are time-dependent, e.g. by a modulation or abrupt change of cooling or heating. In this case, the basic conductive temperature distribution is time-dependent, and the stability problem becomes a non-autonomous one, i.e. the solution cannot in general be sought in the form of exponentials $\exp(\sigma t)$. For time-periodic modulation of the basic state one can resort to Floquet theory (Rosenblat & Tanaka 1971; Bhadauria & Bathia 2002) but, in the general case, the formulation and prediction of critical conditions for the onset of convection becomes much less clear-cut than for a steady base state. The following two basic approaches are common for a general time-dependent basic state:

(i) reduction to an autonomous problem by the *frozen-time assumption*, whereby the basic state is supposed to evolve much more slowly than the perturbations, and

(ii) solution of the full non-autonomous linear perturbation problem for some initial conditions which are supposed to be representative. This is called *amplification theory* (AT).

Both approaches go at least back to the 1960s. The first one was used by Lick (1965) and Currie (1967) and the second by Foster (1965). Later work by Homsy (1973) introduced energy stability ideas, but the resulting bounds are not necessarily useful for predicting instability thresholds and the mathematics is considerably more involved. In each of these works the focus was on buoyancy-driven convection.

The frozen-time approach was used for the Marangoni convection by Kang & Choi (1997). These authors studied the dynamics of a fluid layer subjected to a sudden change in surface temperature. However the frozen-time method was only applied for late times in the evolution. For early times they formulated the so-called propagation theory, whereby the problem is again reduced to an autonomous one by using a certain similarity solution for base state and perturbations. This approximation is actually appropriate for an infinite layer. The frozen-time model relies on the validity of the assumption of fast instability development (relative to the base state). This could be inadequate at instability thresholds, at which the instability can develop on the same time scales as the base state. The other method, namely the amplification model, has a sounder mathematical foundation, but comes with the necessity of identifying representative initial conditions and amplification levels for the perturbations.

A specific analysis suitable for transient problems is developed in this paper, which is an extension of the previous amplification model. The underlying concept is called the non-normal approach. In such a case, the choice of initial perturbations is not somewhat arbitrary as in AT but it is guided by an optimization technique. This procedure consists in identifying, for a given time t and a given wavenumber k, the initial perturbation with the strongest amplification (called the optimal perturbation). Hence this method may exhibit initial conditions which are not *a priori* obvious configurations. As a consequence it gives the maximal value for the perturbation norm that was previously defined for the problem under study. This cannot be achieved through an AT simulation. This has been previously noted by Rapaka *et al.* (2008), who report an optimal perturbation analysis of density-driven convection in porous media. However, their optimization method differs considerably from the adjoint-based method presented here. Concerning the determination of initial conditions, we note that the non-normal approach has also been used for instability problems of steady base flow, e.g. in parallel shear flows, such as boundary layers (Schmid & Henningson 2001) or plane Poiseuille flow (Reddy *et al.* 1998). For such problems, there was a long-standing gap between the standard two-dimensional

Tollmien–Schlichting modes obtained using the classical normal mode analysis – though these modes were only observed in some very controlled experiments – and the general experimental observation of streak generation. It is by resorting to non-normal mode analysis that the coherent structures observed in boundary layer transition, i.e. streamwise rolls and streaks, could be deduced from an optimal approach and their generation linked to the lift-up mechanism proposed by Landahl (Schmid & Henningson 2001).

The non-normal approach can be extended to transient cases. This is precisely what we propose here. Such a method provides the strongest amplification, i.e. the optimal growth at a given duration T after initial conditions have started their evolution. If this amplification is sufficiently large, the optimal perturbations may result in the modification of the basic flow at time T and we can speak of an unstable regime in a way to be defined by a norm. To the best of our knowledge, this approach is the only one capable to provide clear-cut answers on instability problems for truly unsteady basic flows. However, as mentioned by one referee, this definition of the stability condition is blurred owing to a certain arbitrariness in choosing the norm and defining the critical amplification gain. This is inherent to any unsteady linear stability problem and does not depend on the particular method. It is then more suitable to view the results as the estimation of a transition region between a domain exhibiting strong convection and a domain where initial perturbations are damped or have no time to significantly develop during the transient regime. The non-normal approach allows one to characterize this transition domain properly. The results presented here for different norms and different critical amplification values show that this transition region is thin, so that the notion of stability threshold is still valid for this transient problem. On the contrary, the frozen-time assumption may fail, for instance if the base state evolves on the same time scale or faster then the unstable modes characterizing its frozen-time stability. In that case, the computed growth rates might not correspond to any true amplifications, at the system time scale. This might affect the determination of critical conditions since in the frozen-time assumption, the critical conditions are determined using the quasi-static growth rates $\sigma(t)$. However the pertinent character of this method strongly depends on the rapid variation of these 'quasi-static growth rates' with the basic state changes. For instance, the amplification between times t_1 and t_2 would be, at zeroth-order Wentzel–Kramers–Brillouin theory, equal to $\int_{t_1}^{t_2} \sigma(t)\mathrm{d}t$. So if the instantaneous growth rate strongly varies during this interval, its positive value at a given moment may not be interpreted in the right way.

In the present work, we provide the results obtained by means of the non-normal approach as well as the frozen-time approach. In the specific flow case presented here, the quasi-static method is shown to provide similar results except for some particular quantities.

The proposed analysis is general and can be easily extended to many other unsteady problems, e.g. chemically driven hydrodynamic instabilities (Eckert, Acker & Shi 2004). In the present paper, we determine the onset of convection in a drying experiment, which leads to an unsteady Rayleigh–Bénard–Marangoni problem. More specifically we study the sudden cooling due to evaporation of a liquid layer, where the decrease of surface temperature is induced by the vaporization latent heat. This problem has been the subject of many experimental or theoretical studies (see e.g. Berg, Boudart & Acrivos 1966; Vidal & Acrivos 1968, and more recently Mancini & Maza 2004 or Moussy, Lebon & Margerit 2004). The specific motivation for our work is the drying process studied in experiments by Toussaint *et al.* (2008) performed on a polymer solution (polyisobutylene/toluene). The solution initially at the ambient temperature is poured in a dish located in an extractive hood. When evaporation

of toluene begins, convective patterns are observed at the very beginning of the experiment (quasi-instantaneous or less than 100 s after pouring the solution). They disappear well before the end of the drying. The very large Lewis number $Le = \kappa/D_{mol}$ (κ and D_{mol} denote the thermal and mass diffusivity) of the polymer solution (about 10^3) is an indication that the thermal diffusion is faster and that convective patterns observed in the first minutes should be mainly driven by thermal effects. Two experimental observations detailed in Toussaint *et al.* (2008) support this thesis. First, a few experiments were conducted with deuterated solvent, whose density is higher than the polymer density. In that case, the density of the solution decreases when the polymer concentration increases, leading to a stable situation if the solutal Rayleigh–Bénard problem is considered. Since no differences were found with the experiments conducted with the standard solvent, we can exclude solutal buoyancy as a dominant mechanism. Second, free surface temperature fields measured by infrared camera showed that the end of free convection was related to the duration of the transient thermal regime. In these free convection experiments it can be inferred, from the work on steady convection by Pearson (1958), that the Marangoni effect is dominant for thicknesses typically less than 1 cm and the buoyancy dominant for higher thicknesses. For a more accurate description of the experiments see Toussaint *et al.* (2008).

The paper is organized as follows. In §2, we present the basic assumptions of the model and the governing equations. Thereafter the unsteady basic state is described and a specific stability analysis is introduced in §3. In particular, the non-normal method is explained and the choice of norms is discussed. Section 4 contains the main numerical findings for the two limiting situations: the pure Rayleigh–Bénard and the pure Marangoni case. Critical conditions for the optimal modes are presented. Part of these numerical results are also obtained by a scaling analysis. A comparison of this method with the frozen-time approach is also performed. Finally, in §5, the comparison with experimental results is discussed.

2. Mathematical model

2.1. *Basic assumptions of the model*

The mathematical model of Rayleigh–Bénard–Marangoni convection used throughout this paper is based on a one-layer model in which three assumptions are made: (i) the upper surface remains planar, (ii) the layer thickness d remains constant and (iii) the heat and mass fluxes across the upper surface are given by transfer coefficients. Moreover our analysis is restricted to fluids characterized by a Prandtl number $Pr = \nu/\kappa \geqslant 1$ with ν the kinematic viscosity. This turns out to be the case of most liquids (including water and organic solvents). In that instance, the thermal diffusion time scale is always larger than the viscous diffusion time scale.

The first hypothesis can be tested as follows. Two modes of instability are known to occur in the Bénard–Marangoni problem (Scriven & Sternling 1964; Reichenbach & Linde 1981; Goussis & Kelly 1990). One is generated from the interaction of the velocity perturbations with the basic temperature, while the other mode, characterized by a wavelength long compared with the layer thickness, is due to the coupling of the Marangoni effect with the deflection of the free surface. Mathematically, surface deformation can be neglected on scales of order d when the Laplace pressure associated with a curvature $1/d$ is large compared with the dynamic pressure. This condition (Davis 1987) corresponds with the smallness of the crispation number $Cr \equiv (\rho\nu\kappa)/(\sigma d)$ where ρ and σ respectively denote fluid density and surface tension. Moreover, the Galileo number $Ga \equiv (gd^3)/(\nu\kappa)$ characterizes the relative importance of gravity (g gravity constant) and diffusion. A large value of the Galileo number

indicates that gravity stabilizes the long-wave mode. The free surface deformation can be neglected if $Cr \ll 1$ and $Ga \gg 1$. Such conditions are shown be satisfied for the experiments considered here.

The second hypothesis can be adopted if $Pe \ll 1$, where the Péclet number $Pe \equiv (d v_{ev})/\kappa$ is defined as the ratio between v_{ev} the interface velocity due to evaporation which is equal to minus the time derivative of $d(t)$, and the thermal velocity scale κ/d. Indeed when $Pe \ll 1$, the surface displacement $v_{ev}\delta_{diff}$ remains negligible compared to the total thickness d during the problem characteristic time, i.e. the diffusion time $\delta_{diff} \equiv d^2/\kappa$. In the experiment (see §5), the Péclet number is smaller than 0.1.

Finally, let us discuss the third assumption. The boundary condition at the free surface results from the coupling between the system and its surroundings. In evaporation experiments, the solvent flux and thus the temperature gradient in the fluid depends on the heat and mass transfer with the ambient air. Several authors have developed numerical or theoretical studies taking into account this coupling (see e.g. Colinet *et al.* 2003; Merkt & Bestehorn 2003; Moussy *et al.* 2004; Ozen & Narayanan 2004). In this paper we adopt a simple description by global heat and mass transfer coefficients, as our main interest is directed on the transient character of the problem under study and not on the detailed description of the transfer per se.

2.2. *Governing equations*

We formulate the basic equations in a Cartesian coordinate system, where the bottom of the layer coincides with the plane $z = 0$ and the upper free surface with $z = d$. The fluid is characterized by a density ρ, a kinematic viscosity ν, a thermal diffusivity κ and a thermal expansion coefficient α. The Boussinesq approximation is assumed to govern the velocity field $\boldsymbol{v} = v_x \boldsymbol{e}_x + v_y \boldsymbol{e}_y + v_z \boldsymbol{e}_z$ and temperature field T:

$$\frac{\partial \boldsymbol{v}}{\partial t} + (\boldsymbol{v} \cdot \nabla)\boldsymbol{v} = -\frac{\nabla p}{\rho} + \nu \nabla^2 \boldsymbol{v} + g\alpha(T - T_\infty)\boldsymbol{e}_z, \quad \nabla \cdot \boldsymbol{v} = 0, \tag{2.1}$$

$$\frac{\partial T}{\partial t} + (\boldsymbol{v} \cdot \nabla)T = \kappa \nabla^2 T, \tag{2.2}$$

where g denotes the acceleration due to gravity and T_∞ the temperature of the ambient air. In this approximation, the density ρ is taken to be the density at $T = T_\infty$. At the bottom, the velocity satisfies the no-slip condition and the wall is assumed adiabatic since, in the experiment, the bottom of the dish is thermally insulated by an air gap.

$$\boldsymbol{v} = 0, \qquad \partial_z T = 0 \quad \text{at } z = 0. \tag{2.3}$$

The upper boundary conditions are more involved. Assuming a planar surface, the local evaporation mass flux reads

$$Q_m\left(T_s(x, d, t)\right) = \rho \left(v_z(x, d, t) - \frac{\mathrm{d}}{\mathrm{d}t}(d) \right). \tag{2.4}$$

Moreover the global mass balance reads (no fluid is introduced to counterbalance the evaporation mass loss)

$$\bar{Q}_m = -\rho \frac{\mathrm{d}}{\mathrm{d}t}(d) = \rho v_{ev}, \tag{2.5}$$

where $\bar{Q}_m$ is the mean evaporation flux over the free surface. From relations (2.4) and (2.5) we get:

$$v_z = \frac{Q_m(T_s) - \bar{Q}_m}{\bar{Q}_m} v_{ev}. \tag{2.6}$$

If we assume that the flux variations $Q_m(T_s(x, d, t)) - \bar{Q}_m$ are much smaller than the flux $\bar{Q}_m$ itself, then $|v_z| \ll v_{ev} \equiv Pe \, \kappa/d$, the Péclet number being defined using the evaporation velocity (see §2.1). Since $Pe \ll 1$ and κ/d is the velocity scale, the kinematic boundary condition so reduces to

$$v_z = 0 \quad \text{at } z = d. \tag{2.7}$$

In addition, the balance of tangential forces at the upper surface requires that the velocity field satisfies

$$\rho v \partial_z v_j = \partial_j \sigma(T_s), \quad (j = x, y) \quad \text{at } z = d, \tag{2.8}$$

where T_s denotes the temperature inside the fluid layer at $z = d$ and $\sigma(T)$ denotes the surface tension which is assumed to be a linearly decreasing function of temperature,

$$\sigma(T) = \sigma(T_\infty) - \gamma(T - T_\infty), \quad \gamma \equiv -\frac{d\sigma}{dT} > 0. \tag{2.9}$$

Finally, the conservation of energy flux should be imposed at the interface. It reads

$$-\lambda \frac{\partial T}{\partial z} + h_{th}(T_\infty - T_s) = L Q_m(T_s) \tag{2.10}$$

The first left-hand side term represents the heat conduction in the liquid, λ denoting the thermal conductivity related to the thermal diffusivity *via* $\lambda = \kappa \rho C$ with C the liquid specific heat. The second left-hand side term expresses the heat flux density in the gas using a simple phenomenological model based on the heat transfer coefficient h_{th} and the difference between the air temperature T_∞ far from the liquid and the surface temperature T_s. Finally, the cooling effect due to solvent vaporization is expressed in the right-hand side term, where L stands for the latent heat of vaporization and Q_m for the solvent mass flux per unit area. This latter quantity depends on the surface temperature T_s. In the framework of the one-layer model, one imposes

$$Q_m(T_s) = h_m(c_s(T_s) - c_\infty), \tag{2.11}$$

where c_s and c_∞ denote the solvent concentration in the gas phase near the surface and far from the surface, respectively, and h_m is the phenomenological mass transfer coefficient in the gas. Assuming local thermodynamic equilibrium, c_s directly depends on the surface temperature through the saturated vapour pressure. The variable Q_m can be linearized around T_∞ which leads to the final expression:

$$-\lambda \frac{\partial T}{\partial z} + H_{th}(T_\infty - T_s) = L Q_m(T_\infty), \quad H_{th} = h_{th} + L \frac{\partial Q_m}{\partial T}(T_\infty). \tag{2.12}$$

Initially, the liquid layer is isothermal, i.e. $T(z, t = 0) = T_\infty$. At large times, the system reaches a steady state in which the temperature in the layer is again uniform but with a temperature difference $T_\infty - T_s = \Delta T_{st} > 0$ with the gas located far from the surface. This difference is imposed by the condition (2.12), where

$$\Delta T_{st} \equiv \frac{L Q_m}{H_{th}}. \tag{2.13}$$

To put the above equations in a non-dimensional form, scales for temperature, length, velocity and time are needed. The temperature difference ΔT_{st} provides the temperature scale and the layer thickness d the relevant length scale. Two velocity scales can be introduced in this problem namely the viscous velocity scale $V = \nu/d$ and the thermal velocity scale $V = \kappa/d$. Here only the thermal scale $V = \kappa/d$ is used.

Finally, the appropriate time scale is the thermal diffusion time $d/V = d^2/\kappa$. The non-dimensionalization leads to equations for v and $\theta(z,t) = (T(z,t) - T_\infty)/\Delta T_{st}$:

$$\frac{1}{Pr}(\partial_t v + (v \cdot \nabla)v) = -\nabla p + \nabla^2 v + Ra\theta e_z, \tag{2.14}$$

$$\nabla \cdot v = 0, \tag{2.15}$$

$$\partial_t \theta + (v \cdot \nabla)\theta = \nabla^2 \theta, \tag{2.16}$$

$$\partial_z v_x + Ma\,\partial_x \theta = \partial_z v_y + Ma\,\partial_y \theta = 0 \quad \text{at } z = 1. \tag{2.17}$$

$$\partial_z \theta + Bi\,\theta + Bi = 0 \quad \text{at } z = 1, \quad \partial_z \theta = 0 \quad \text{at } z = 0, \tag{2.18}$$

$$v_z = 0, \quad \text{at } z = 1 \quad v_x = v_y = v_z = 0 \quad \text{at } z = 0. \tag{2.19}$$

in which the Rayleigh, Marangoni, Prandtl and Biot numbers

$$Ra = \frac{\alpha g d^3 \Delta T_{st}}{\nu\kappa}, \quad Ma = \frac{\gamma d \Delta T_{st}}{\rho\nu\kappa}, \quad Pr = \frac{\nu}{\kappa}, \quad Bi = \frac{H_{th}d}{\lambda} \tag{2.20}$$

appear.

In the following, we discriminate between two opposite cases: $Bi \ll 1$ or $1 \ll Bi$. This corresponds respectively to an effective conductance H_{th} in the gas much smaller or much larger than the heat conductance λ/d in the fluid.

3. Basic state and optimal linear perturbations

We study the stability of a purely conductive unsteady basic state $\theta_0(z,t)$ which is initially uniform, i.e. $\theta_0(z, t=0) = 0$. This state evolves since the upper free surface is cooled down by the latent heat released through evaporation: The velocity field remains always zero but the unsteady field $\theta_0(z,t)$ satisfies a pure heat equation

$$\frac{\partial\theta_0}{\partial t} = \frac{\partial^2\theta_0}{\partial z^2} \quad \text{with} \quad \partial_z \theta_0 = 0 \quad \text{at } z = 0, \quad \partial_z \theta_0 + Bi\,\theta_0 + Bi = 0 \quad \text{at } z = 1. \tag{3.1}$$

The basic state only depends on the Biot number Bi. Note that the term $Bi\theta_0$ characterizes the heat transfer in the gas phase and the term Bi represents the cooling effect due to evaporation. The unsteady temperature field $\theta_0(z,t)$ is shown in figure 1 for different Biot numbers and times. A cooled layer develops from the upper surface whose thickness $\delta_0(t) \sim \min(\sqrt{t}, 1)$ is similar at a given time for different Biot numbers and increases until it fills the whole layer. Conversely, if $\Delta\theta_0(t)$ denotes the characteristic temperature difference within the fluid, the maximum reached over the whole time evolution by this quantity increases with Biot number Bi (figure 1d). Actually, two different regimes are observed according to the value of Bi (see Appendix A of the supplementary material available at journals.cambridge.org/flm). For small Biot numbers, typically $Bi \lesssim 1$, the cooled layer reaches the bottom while the jump $\Delta\theta_0(t)$ is less than 1. Afterwards, $\Delta\theta_0(t)$ decreases. Such time evolution can be summarized by the following scalings:

$$|\theta_0| \sim \Delta\theta_0 \sim Bi\sqrt{t}, \quad \delta_0(t) \sim \sqrt{t} \quad \text{for} \quad 0 \lesssim \sqrt{t} \lesssim 1, \tag{3.2}$$

$$|\theta_0| \sim Bi\,t, \quad \Delta\theta_0(t) \sim Bi, \quad \delta_0(t) \sim 1 \quad \text{for} \quad 1 \lesssim t \lesssim Bi^{-1}, \tag{3.3}$$

For $Bi^{-1} \lesssim t$, the temperature field θ_0 relaxes towards the steady uniform temperature $\theta_0(z,t) = -1$ and all the energy needed by evaporation is carried on by convection in the gas phase.

For large Biot numbers, typically $Bi \gtrsim 10$, the temperature jump $\Delta\theta_0(t)$ reaches a maximum before the cooled layer reaches the bottom (figure 1a). In that case, the
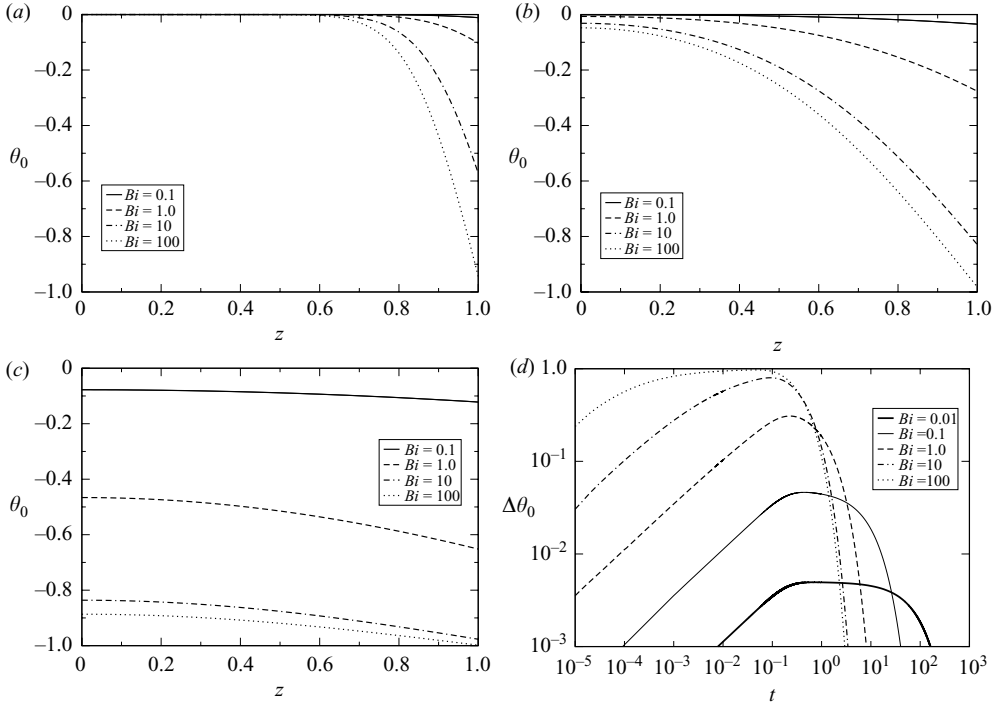
FIGURE 1. Basic temperature profile for different Biot numbers. (a)–(c) Temperature profile at times $t = 10^{-2}$, $t = 10^{-1}$ and $t = 1$. (d) Temperature difference $\Delta\theta_0(t)$ as a function of time t.

maximal jump is equal to one and $|\theta_0(z=1, t)| \sim 1$ at that time. The time evolution can be summarized by the following scalings:

$$|\theta_0| \sim \Delta\theta_0 \sim Bi \sqrt{t}, \quad \delta_0(t) \sim \sqrt{t} \quad \text{for} \quad 0 \lesssim t \lesssim Bi^{-2}, \tag{3.4}$$

$$\Delta\theta_0 \sim 1, \quad \delta_0 \sim \sqrt{t} \quad \text{for time} \quad Bi^{-2} \lesssim t \lesssim 1. \tag{3.5}$$

For $1 \lesssim t$, the temperature decreases in the whole layer thickness to reach the steady state regime $\theta_0(z, t) = -1$.

In order to study the stability of the unsteady conductive state we split the fields into a basic flow and three-dimensional perturbations

$$\boldsymbol{v} = \boldsymbol{v}_p(x, y, z, t), \quad \theta = \theta_0(z, t) + \theta_p(x, y, z, t), \quad p = p_0(z, t) + p_p(x, y, z, t) \tag{3.6}$$

and linearize in the perturbations to get a set of linear equations. Since this problem has no preferential direction in the (x, y) plane, the perturbation Fourier modes in such directions decouple in the linear regime. Without loss of generality, we thus consider a non-dimensional wavenumber k in the x direction and no dependence in the y direction reducing the flow to be two-dimensional:

$$(\boldsymbol{v}_p, \theta_p, p_p) = (\hat{u}(z, t), 0, \hat{w}(z, t), \hat{\theta}(z, t), \hat{p}(z, t)) \exp(\mathrm{i}kx). \tag{3.7}$$

These infinitesimal perturbations are governed by the linear system

$$\frac{1}{Pr} \frac{\partial}{\partial t} \hat{u} + \mathrm{i}k\hat{p} - \left[\frac{\partial^2}{\partial z^2} - k^2 \right] \hat{u} = 0, \tag{3.8}$$

$$\frac{1}{Pr}\frac{\partial}{\partial t}\hat{w} + \frac{\partial\hat{p}}{\partial z} - \left[\frac{\partial^2}{\partial z^2} - k^2\right]\hat{w} - Ra\hat{\theta} = 0, \quad ik\hat{u} + \frac{\partial\hat{w}}{\partial z} = 0, \tag{3.9}$$

$$\frac{\partial}{\partial t}\hat{\theta} + \hat{w}\frac{\partial\theta_0}{\partial z} - \left[\frac{\partial^2}{\partial z^2} - k^2\right]\hat{\theta} = 0, \tag{3.10}$$

$$\hat{w} = 0, \quad \partial_z\hat{u} + Ma\, ik\hat{\theta} = 0, \quad \partial_z\hat{\theta} + Bi\,\hat{\theta} = 0, \quad \text{at } z = 1, \tag{3.11}$$

$$\hat{u} = \hat{w} = 0, \quad \frac{\partial\hat{\theta}}{\partial z} = 0 \quad \text{at } z = 0. \tag{3.12}$$

To quantify the amplification gain at time t_1, it is customary to define a norm which is generally based on the kinetic energy of perturbations. This norm can be orthogonally decomposed in a Fourier basis so that the individual contributions of each wavenumber k can be studied independently. In the present case, the temperature field is playing a major role as well. We thus define two different norms corresponding to two different situations. The first one is based on the kinetic energy of perturbations

$$E_V(t_1) \equiv \int (\hat{u}(z, t_1)\hat{u}^+(z, t_1) + \hat{w}(z, t_1)\hat{w}^+(z, t_1))\,dz, \tag{3.13}$$

where superscript $+$ denotes complex conjugation. The integration is performed over the entire layer width and perturbations are obtained after integrating the above linear system over the time period $[0, t_1]$. The second one

$$E_T(t_1) \equiv \int \hat{\theta}(z, t_1)\hat{\theta}^+(z, t_1)\,dz \tag{3.14}$$

is based on the temperature field and not on the velocity field.

For finite Prandtl number two extreme cases are considered, with the initial perturbation concerning either the velocity field, or the temperature field. In the following we will consider the amplification factors $E_V(t_1)/E_V(0)$ or $E_T(t_1)/E_T(0)$ to characterize the stability. Then, when the initial perturbations only concern the velocity field, we only take into account the amplification $E_V(t_1)/E_V(0)$ since $E_T(0) = 0$. Conversely, when the initial perturbations only concern the temperature field we use the amplification factor $E_T(t_1)/E_T(0)$. For the infinite Prandtl number case, the velocity perturbations are not dynamical quantities since the time derivative of the velocity drops out from (3.8)–(3.9). In other words, the velocity perturbations are slaved to the temperature perturbations. In this case, we use only $E_T(t_1)/E_T(0)$ and hence the norm E_T.

For a given initial disturbance, one evaluates the amplification gain at time t_1 by computing $E(t_1)/E(0)$ where $E = E_V$ or $E = E_T$. It is the purpose of a non-normal analysis to compute the quantity $\hat{G}(t_1; k; Ma, Ra, Bi, Pr) \equiv \max[E(t_1)/E(0)]$ which is the upper bound for the energy amplification that a disturbance of wavenumber k can reach at time t_1. This approach solves a sort of the finite time stability problem: it investigates the transient evolution and defines for any time t_1, an optimal perturbation mode which actually reaches the upper bound (Schmid & Henningson 2001). This mode (i.e. the optimal initial z profile) is found numerically by solving an optimization problem (Farrell & Ioannou 1996; Andersson, Berggren & Henningson 1999; Luchini 2000; Schmid & Henningson 2001). The optimum of $E(t_1)$ is determined taking into account several constraints: (i) the disturbance energy at time $t = 0$ is equal to unity; (ii) the disturbance satisfies the linear governing equation as well as the boundary conditions during the complete time interval $[0, t_1]$. This problem is best solved with the help of a Lagrangian formalism and Lagrangian multipliers which are introduced

to precisely enforce the above constraints. In the present case, these multipliers are adjoint fields $(\tilde{u}(z,t), \tilde{w}(z,t), \tilde{\theta}(z,t), \tilde{p}(z,t))$. Following a standard derivation, these quantities satisfy a set of adjoint equations. It is

$$\frac{1}{Pr}\frac{\partial}{\partial\tau}\tilde{u} - \mathrm{i}k\tilde{p} - \left[\frac{\partial^2}{\partial z^2} - k^2\right]\tilde{u} = 0, \tag{3.15}$$

$$\frac{1}{Pr}\frac{\partial}{\partial\tau}\tilde{w} - \frac{\partial\tilde{p}}{\partial z} - \left[\frac{\partial^2}{\partial z^2} - k^2\right]\tilde{w} + \tilde{\theta}\frac{\partial\theta_0}{\partial z} = 0, \quad \mathrm{i}k\tilde{u} + \frac{\partial\tilde{w}}{\partial z} = 0, \tag{3.16}$$

$$\frac{\partial}{\partial\tau}\tilde{\theta} - \left[\frac{\partial^2}{\partial z^2} - k^2\right]\tilde{\theta} - Ra\tilde{w} = 0, \tag{3.17}$$

$$\tilde{u} = \tilde{w} = 0, \quad \frac{\partial\tilde{\theta}}{\partial z} = 0 \quad \text{at } z = 0, \tag{3.18}$$

$$\tilde{w} = 0, \quad \partial_z\tilde{u} = 0, \quad \partial_z\tilde{\theta} + Bi\,\tilde{\theta} + Ma\,\partial_z\tilde{w} = 0 \quad \text{at } z = 1, \tag{3.19}$$

in which $\tau \equiv -t$. These adjoint equations have to be solved backwards in time. Let us denote by the symbol $\boldsymbol{q}$ the vector field (u, w, θ, p). One obtains the optimal perturbation for time t_1 by an iterative scheme which propagates a given initial condition forwards in time using the direct problem (here denoted by $F_j(\boldsymbol{q}) = 0$, $j = 1\ldots 4$), the result of which serves as an 'initial' condition for the backward propagation by the adjoint equations (here denoted by $\tilde{F}_j(\tilde{\boldsymbol{q}}(t)) = 0$, $j = 1\ldots 4$). More specifically (see Appendix B of the supplementary material available at journals.cambridge.org/flm), a relation between the adjoint $\tilde{\boldsymbol{q}}(z, t_1)$ and $\boldsymbol{q}(z, t_1)$ is imposed. After one forward–backward integration, quantity $\tilde{\boldsymbol{q}}(z, 0)$ is obtained and a relation between $\tilde{\boldsymbol{q}}(z, 0)$ and $\boldsymbol{q}(z, 0)$ is also imposed. An updated initial condition for the next iterative step is then available. This process should be self-consistent: one uses an iteration procedure which is schematically illustrated by a diagram

$$
\begin{array}{ccc}
\boldsymbol{q}(z, 0) & \xrightarrow{F_j(\boldsymbol{q})=0} & \boldsymbol{q}(z, t_1) \\
\uparrow & & \downarrow \\
\tilde{\boldsymbol{q}}(z, 0) & \xleftarrow{\tilde{F}_j(\tilde{\boldsymbol{q}})=0} & \tilde{\boldsymbol{q}}(z, t_1)
\end{array} \tag{3.20}
$$

Convergence is reached when the initial condition for the forward problem does not change appreciably – up to a normalization constant – by an appropriately chosen criterion from one iterative step to the next. The converged mode is precisely the initial optimal perturbation for time t_1. The maximum energy amplification is computed by propagating the converged initial condition forwards in time and by forming the ratio of the disturbance energy at the end of the time interval to the energy at the beginning. The direct and adjoint equations have been discretized using a pseudospectral method based on Chebyshev polynomials and a streamfunction-based formulation to account for incompressibility (see Appendix C of the supplementary material available at journals.cambridge.org/flm).

4. Numerical results

4.1. *Quantities provided by the non-normal analysis*

For the unsteady basic state $\theta_0(z, t)$, a given set (Ma, Ra, Bi, Pr) and a given type of initial perturbation (temperature or velocity), the non-normal analysis determines at a given time t_1, the maximum energy amplification $\hat{G}(t_1; k; Ma, Ra, Bi, Pr)$ over all possible perturbations of wavenumber k (see figure 2). In a way, the value $\ln\hat{G}/t_1$ is analogous to a growth rate for classical stability analysis. More generally, it
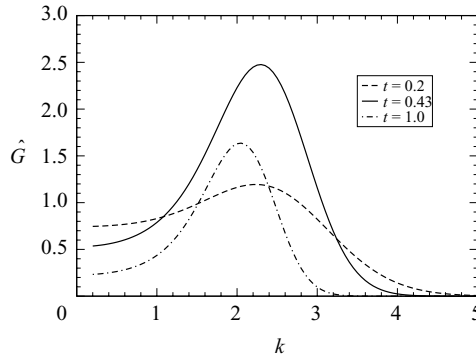
FIGURE 2. The maximum energy amplification $\hat{G}(t;k;Ma,Ra,Bi,Pr)$ as a function of wavenumber k for three different times $t=0.2$, $t=0.43$ and $t=1$. Parameters $Ma=300$, $Ra=0$, $Bi=1$, $Pr=\infty$.
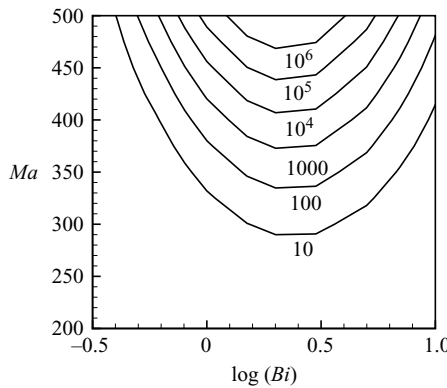

FIGURE 3. Isolines of the maximum amplification $G_{max}(Ma,Ra,Bi,Pr)$ in the plane (Bi,Ma) Parameters $Ra=0$, $Pr=\infty$. The values of the isolines are written on the figure.

appears possible to extend the usual concepts of classical stability analysis to unsteady flows. For instance, $\hat{G}(t_1;k;Ma,Ra,Bi,Pr)$ can be maximized over wavenumber k and time t_1 providing the global maximum amplification $G_{max}(Ma,Ra,Bi,Pr)$ (see figure 3). This value is reached at time $t=t_{opt}(Ma,Ra,Bi,Pr)$, for an optimal wavenumber denoted by $k_{opt}(Ma,Ra,Bi,Pr)$ and for a specific perturbation structure in z. These latter two quantities play the role of the most amplified wavenumber and of the most amplified mode for the standard stability analysis. One also obtains a 'stability' diagram, by determining the region of the space (Bi,Pr,Ma,Ra) where the amplification gets above a threshold G_{thres}. It is a way of separating the region where amplification or attenuation occurs. The value of G_{thres}, for instance $G_{thres}=1$, is somewhat arbitrary: as already said in the introduction, an unsteady problem is indeed characterized more by a transition domain than a well-defined threshold. It is demonstrated below that choosing $G_{thres}=1$ or $G_{thres}=100$ does not result in major differences, so that the transition region is thin compared with the absolute values of the Marangoni and Rayleigh numbers. For fixed Ra and Pr, one can determine the curve $Ma_c(Bi,Ra,Pr)$ such that if $Ma<Ma_c$ and $Ma>Ma_c$ then $G_{max}<G_{thres}$ and $G_{max}>G_{thres}$, respectively. Similarly, one may define for fixed Ma and Pr, the curve $Ra_c(Bi,Ma,Pr)$. These curves play a role very much similar to marginal stability curves. Each point of the critical curve is associated to a critical wavenumber $k_c \equiv k_{opt}$
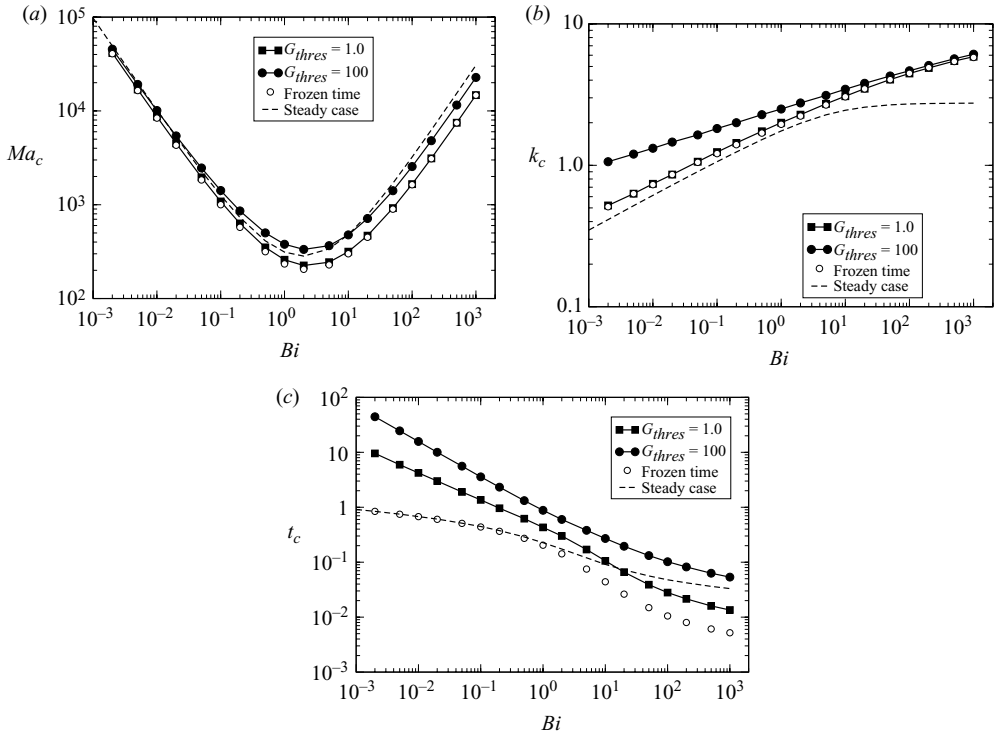
FIGURE 4. Infinite Prandtl number case and $Ra = 0$. Results are shown for two thresholds $G_{thres} = 1$ and $G_{thres} = 100$. Frozen-time and steady state results are presented for comparison (see text for details). (a) Critical Marangoni $Ma_c(Bi)$, (b) critical wavenumber $k_c(Bi)$, (c) critical time $t_c(Bi)$.

and critical optimal time $t_c \equiv t_{opt}$. Note that until this point, most of this procedure can be extended to other unsteady problems in a straightforward way. A comparison between these critical curves and the experimental diagram, which separates the domains where convection is observed or not observed, is made in §5.

4.2. *Infinite Prandtl number: the pure Marangoni case $Ma \neq 0$ and $Ra = 0$*

For infinite Prandtl number, the velocity is slaved to the temperature field. As a consequence, only perturbations in temperature field are pertinent. In the plane (Bi, Ma), the critical curve $Ma_c(Bi)$, critical wavenumber $k_c(Bi)$ and critical optimal time $t_c(Bi)$ are presented for the pure Marangoni case and two thresholds $G_{thres} = 1$ and $G_{thres} = 100$ (figure 4). The critical Marangoni number $Ma_c(Bi)$ slightly depends on the value of the threshold and seems to be consistent, within the numerical uncertainties, to the following laws (here $G_{thres} = 1$):

$$Ma_c(Bi) \simeq 83/Bi \quad \text{for} \quad Bi \ll 1 \quad \text{and} \quad Ma_c(Bi) \simeq 15Bi \quad \text{for} \quad 1 \ll Bi. \quad (4.1)$$

Moreover the wavenumber $k_c(Bi)$ (figure 4b) is an increasing function of the Biot number while optimal time $t_c(Bi)$ is a decreasing function of the same parameter.

Using heuristic arguments (cf. Appendix D available with the online version of the paper), the following scaling laws can be deduced:

For $Bi \ll 1$ the critical conditions for instability can be expressed as

$$Ma_c \sim 1/Bi \quad \text{with} \quad \sqrt{Bi} \lesssim k_c \lesssim 1 \quad \text{and} \quad 1 \lesssim t_c \lesssim 1/Bi. \quad (4.2)$$
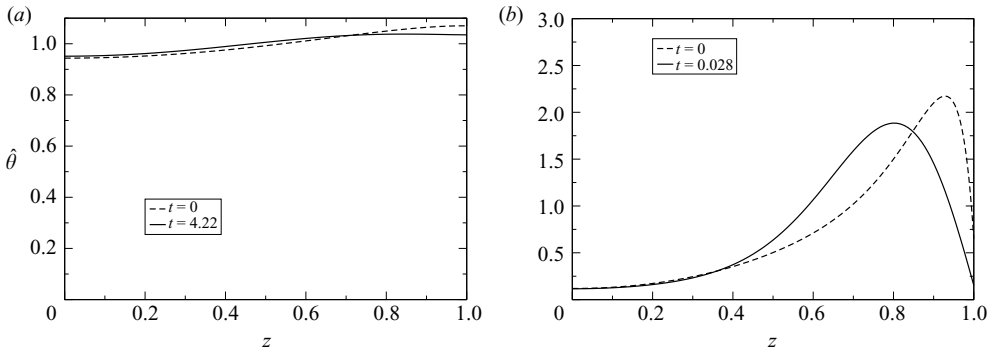
FIGURE 5. The optimal temperature perturbation $\hat{\theta}(z, t)$ at time $t = 0$ (dashed) and $t = t_c$ (solid) for $Ra = 0$, $Pr = \infty$, $G_{thres} = 1$: (a) $Bi = 0.01$, $Ma = Ma_c = 8685$ and $k = k_c = 0.74$; (b) $Bi = 100$, $Ma = Ma_c = 1658$ and $k = k_c = 4.46$.

For $1 \ll Bi$, the critical conditions become

$$Ma_c \sim Bi \quad \text{with} \quad 1 \lesssim k_c \lesssim Bi \quad \text{and} \quad t_c \sim k_c^{-2}. \tag{4.3}$$

The spatial structure in z of the optimal perturbation at $k = k_c$ and $Ma = Ma_c$ is shown on figure 5 for two Biot numbers and two different times: time $t = 0$ and time $t = t_c$ when the perturbation reaches its maximum amplification. The spatial structure of this optimal perturbation is shown to change slightly during the time evolution. In this respect, this optimal mode does not differ much from the classical most amplified mode of steady problems.

4.3. *Infinite Prandtl number: the pure Rayleigh case $Ra \neq 0$ and $Ma = 0$*

In the plane (Bi, Ra), the critical curves $Ra_c(Bi)$, $k_c(Bi)$ and $t_c(Bi)$ are presented for two thresholds $G_{thres} = 1$ and $G_{thres} = 100$ (figure 6). The critical Rayleigh number $Ra_c(Bi)$ slightly depends on the value of the threshold and seem to be consistent, within numerical uncertainties, to the following laws (here $G_{thres} = 1$):

$$Ra_c(Bi) \simeq 600/Bi \quad \text{for} \quad Bi \ll 1 \quad \text{and} \quad Ra_c(Bi) \simeq 960 \quad \text{for} \quad 1 \ll Bi. \tag{4.4}$$

Moreover the wavenumber $k_c(Bi)$ and time $t_c(Bi)$ are increasing and decreasing functions, respectively, of the Biot number for small Biot and reach a plateau for larger Biot number.

One can deduce, using heuristic arguments (see Appendix D of the supplementary material available at journals.cambridge.org/flm), the following scaling laws:

$$Ra_c \sim 1/Bi \quad \text{with} \quad \sqrt{Bi} \lesssim k_c \lesssim 1 \quad \text{and} \quad 1 \lesssim t_c \lesssim 1/Bi, \quad \text{for} \quad Bi \ll 1, \tag{4.5}$$

$$Ra_c \sim 1 \quad \text{with} \quad k_c \sim 1 \quad \text{and} \quad t_c \sim 1, \quad \text{for} \quad 1 \ll Bi. \tag{4.6}$$

4.4. *Comparison with classical steady results and with transient frozen-time method*

It is worth comparing the results presented here with the well-known results obtained by Pearson (1958) in the framework of the steady Marangoni problem and Sparrow, Goldstein & Jonsson (1963) in the framework of the steady Rayleigh problem. This comparison is pertinent since the boundary conditions at the top and the bottom of the layer (see (3.11)–(3.12)) are similar in the present work and in these classical analyses. However, the Marangoni and Rayleigh numbers defined by these authors are based on the steady temperature difference ΔT_0 between the top and the bottom of
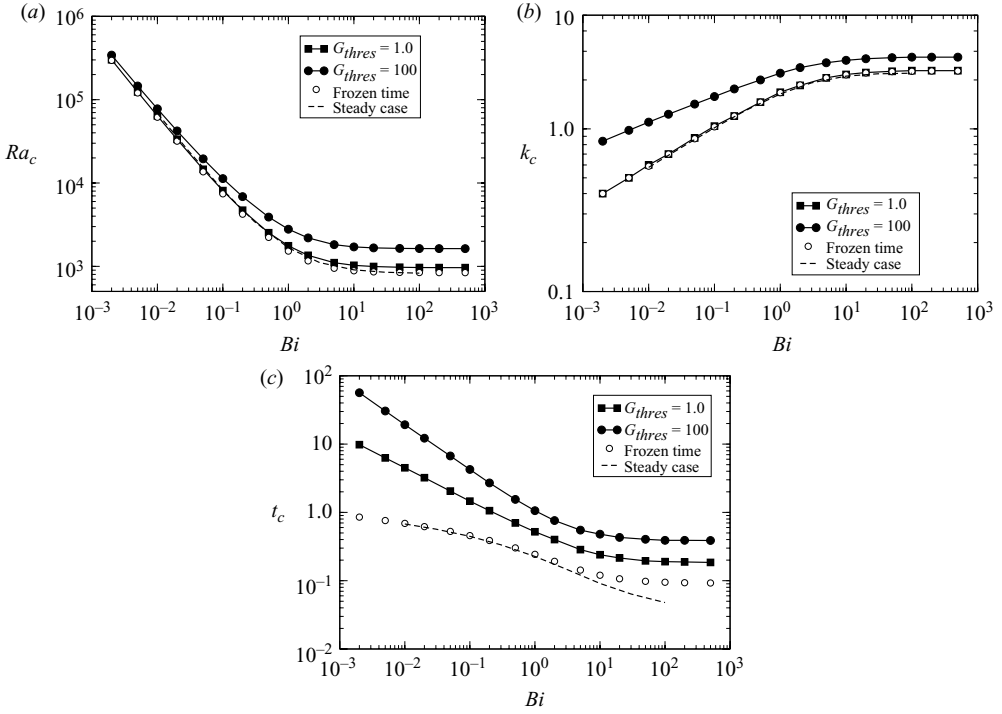
FIGURE 6. Infinite Prandtl number case and $Ma = 0$. Results are shown for two thresholds $G_{thres} = 1$ and $G_{thres} = 100$. Frozen-time and steady state results are presented for comparison (see text for details). (*a*) Critical Rayleigh $Ra_c(Bi)$, (*b*) critical wavenumber $k_c(Bi)$, (*c*) critical time $t_c(Bi)$.

the layer. This steady temperature difference is missing in the transient problem under study. It is then not possible to make a direct comparison between the thresholds values obtained in our paper and the previous ones from Pearson's or Sparrow's publications, and a preliminary transformation is needed. Indeed, at each time t, one might define the equivalent temperature difference between the top and the bottom of the layer, i.e. $\Delta\theta_0(t)\Delta T_{st}$. Using such a temperature difference, it is then easy to define a time-dependent Marangoni $\bar{M}a(t) = \Delta\theta_0(t)Ma$ or a time-dependent Rayleigh numbers $\bar{R}a(t) = \Delta\theta_0(t)Ra$.

Let us compute the maximum of $\Delta\theta_0(t)$ obtained during the time evolution for the Marangoni and Rayleigh cases. This maximum is reached at time t_c and leads to a new Marangoni number $\bar{M}a(t_c)$ and Rayleigh number $\bar{R}a(t_c)$ which can be compared to the critical values $\bar{M}a_{Steady}$ and $\bar{R}a_{Steady}$, respectively, obtained by Pearson (1958) and Sparrow *et al.* (1963), respectively, from the steady case. With the scalings used here, the critical Marangoni Ma_c and Rayleigh Ra_c, respectively, predicted from these steady results read

$$Ma_c \simeq \frac{\bar{M}a_{Steady}}{\Delta\theta_0(t_c)} \quad \text{and} \quad Ra_c \simeq \frac{\bar{R}a_{Steady}}{\Delta\theta_0(t_c)} \tag{4.7}$$

Such estimations have been plotted on figures 4 and 6. They are found to be close to our results for $G_{thres} = 1$. The same comment applies for the critical wavenumbers

except for the Bénard–Marangoni case at high Biot numbers. For critical times, however, the steady-state approximation differs from our results.

When using the results by Pearson (1958) or Sparrow, Goldstein & Jonsson (1963), we are clearly using the normal mode results obtained for a linear temperature field in z on the whole thickness, which is a rough approximation especially at high Biot number. We can go even further and compare the non-normal mode results within the frozen-time approximation. In this latter approximation, a stability analysis in terms of normal modes is performed at each time t. The 'steady' base flow is assumed to be the temperature field $\theta_0(z, t)$ computed at this specific time t. When the flow is stable within this frozen-time approximation for each time t, it will be assumed stable. When the control parameter reaches a critical value (here Ma_c or Ra_c), there exists a unique critical time t_c for which the frozen-time state $\theta_0(z, t_c)$ possesses a marginal eigenvector with a critical wavenumber. In the present problem we have determined the critical parameters for neutral conditions in the frozen-time case by the Lapack routine DGGEV for generalized eigenvalue problems in combination with a Chebyshev collocation method. As can be seen in figures 4 and 6, results for the thresholds and the critical wavenumbers using the non-normal approach ($G_{thres} = 1$) and the frozen-time approximation are close. However the prediction of critical times t_c still differs. In the frozen-time approximation, t_c corresponds to a time when the quasi-static growth rate $\sigma(t)$ becomes zero. This critical time is of a different nature than the critical time for the non-normal approach. The latter characterizes the perturbation evolution over the time interval from $t = 0$ up to t_c. In zeroth-order WKB theory, the critical time t_c for the non-normal approach would be determined by $\int_0^{t_c} \sigma(t) \mathrm{d}t = \ln(G_{thres})$. Suitable modifications of the frozen-time analysis based on this observation should therefore lead to closer agreement regarding the critical times (we do not pursue this issue further in the present work). The frozen-time approximation apparently provides a bound of order unity for t_c because the available temperature difference $\Delta\theta_0(t)$ attains its maximum as soon as the thermal boundary layer of the basic temperature distribution has reached the bottom of the layer. For small Bi, $\Delta\theta_0(t)$ remains fairly constant for larger times, and the instability can develop on this quasi-steady background over fairly long times. This observation can explain the apparently unbounded growth of t_c with Bi for $Bi \to 0$ in the non-normal analysis.

4.5. *Results for finite Prandtl numbers*

In this section, we focus on finite Prandtl numbers and more specifically on the role of initial perturbations on the transition zone estimation. In this case, the velocity field is not slaved to the temperature field so that perturbations in velocity can be considered as well as perturbations in temperature. We only discuss the curves for the pure Marangoni case ($Ra = 0$) (figure 7) but similar results apply to the pure Rayleigh case ($Ma = 0$).

Since the frozen-time approximation seems to be valid for this unsteady problem and an exchange of stability in a normal mode is not affected by the Prandtl number, the effect of this latter number should not be significant. Indeed, for temperature perturbations, the critical Marangoni $Ma_c(Bi, Pr)$ is not affected when infinite Pr number case is compared to $Pr = 10$. For the optimal time $t_c(Bi, Pr)$ and wavenumber $k_c(Bi, Pr)$, the same conclusions apply. For velocity perturbations, the curves differ but not in a drastic way taking into account that perturbations are of a completely different nature compared with the infinite-Prandtl-number problem. Perturbing the temperature is more efficient than perturbing the velocity. Indeed critical Marangoni numbers are smaller for temperature perturbations, but the difference is of the same
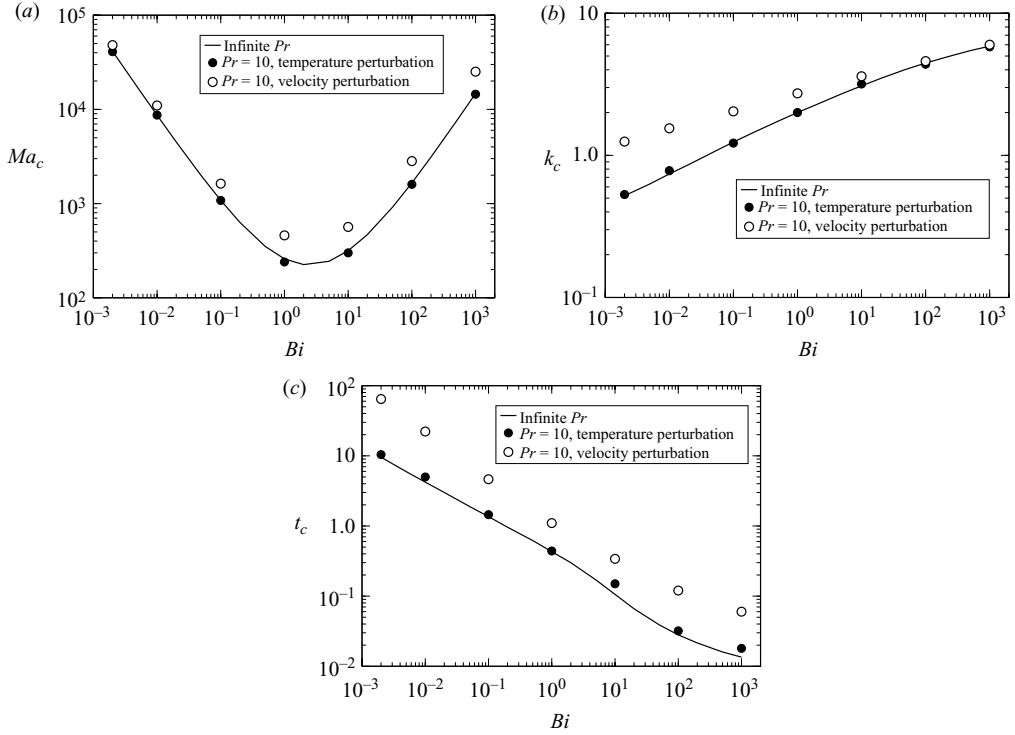
FIGURE 7. Infinite Prandtl ($Pr = \infty$) or finite Prandtl ($Pr = 10$) number cases. Temperature or velocity initial perturbation results with threshold $G_{thres} = 1$. (*a*) Critical Marangoni $Ma_c(Bi)$, (*b*) critical wavenumber $k_c(Bi)$, (*c*) critical time $t_c(Bi)$.

order as the one obtained by changing the threshold value from 1 to 100. Actually, the 'blurriness' of this transient problem induced by the choice of the threshold values and perturbation types is not very broad and does not modify the order of magnitude of the critical numbers if one excepts the time t_c. Finally, let us note that nonlinear direct simulations have also been made to solve this problem (Touazi *et al.*, 2010), showing very good agreement with the linear results presented here.

5. Comparison with experiments

The present section is devoted to the comparison between results obtained from the optimal mode calculations and from an experimental work described in Toussaint *et al.* (2008), where transient Rayleigh–Bénard–Marangoni convection is generated by drying a polymer solution of polyisobutylene-toluene at ambient temperature. In the experiments, buoyancy and Marangoni effects are equally present. It is the evaporation of the solvent, i.e. toluene which cools the upper surface by latent heat. During the experiments, the following parameters are kept constant:

$$\left.\begin{array}{c} \kappa = 0.97 \times 10^{-7} \text{ m}^2 \text{ s}^{-1}, \quad \lambda = 0.142 \text{ W K}^{-1} \text{ m}^{-1}, \quad \rho = 865 \text{ kg m}^{-3}, \\ \alpha = 1.07 \times 10^{-3} \text{ K}^{-1}, \quad \sigma = 28 \times 10^{-3} \text{ N m}^{-1}, \quad \gamma = 1.19 \times 10^{-4} \text{ N K}^{-1} \text{ m}^{-1}, \\ L = 3.96 \times 10^{5} \text{ J kg}^{-1}, \quad H_{th} = 28 \text{ W K}^{-1} \text{ m}^{-2}, \quad \Delta T_{st} = 4.8 \text{ K}. \end{array}\right\} \quad (5.1)$$

Different thicknesses d and dynamic viscosities μ are considered. d is varied from 0.3 mm to 23.5 mm while dynamic viscosity μ is set to a value in the range
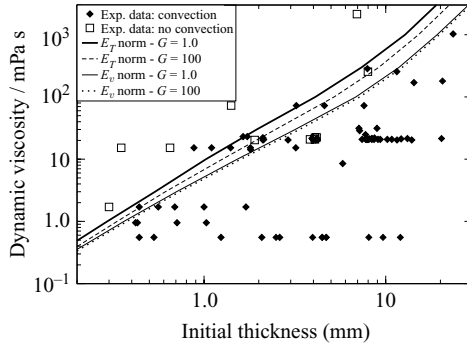
FIGURE 8. Comparison of theoretical and experimental results in the plane (d, μ) where d stands for the layer thickness and μ the dynamic viscosity. The various curves displayed in solid lines correspond to two different thresholds $G_{thres} = 1$, $G_{thres} = 100$ and two different perturbation types (velocity and temperature). Experimental data are displayed by symbols.

[0.55 mPa s, 2100 mPa s] by monitoring the initial polymer concentration. These data allow us to estimate the crispation, the Galileo and the Péclet numbers for each experiment. We get the following bounds for these numbers:

$$10^{-7} \leqslant Cr \leqslant 10^{-3}, \quad 2 \times 10^2 \leqslant Ga \leqslant 3 \times 10^8, \quad 10^{-3} \leqslant Pe \leqslant 0.1. \quad (5.2)$$

As a consequence, the assumption of planar free surface and constant thickness layer are justified. The other relevant non-dimensional numbers vary in the following range:

$$0.06 \leqslant Bi \leqslant 5; \quad 6.6 \leqslant Pr \leqslant 2.5 \times 10^4; \quad 20 \leqslant Ma \leqslant 1.2 \times 10^5; \quad 1.3 \leqslant Ra \leqslant 1.4 \times 10^6. \quad (5.3)$$

The comparison is displayed using the critical dynamic viscosity $\mu_c(d)$ as a function of thickness d (figure 8). In the plane (d, μ), each point corresponds to a given parameter set (Ra, Ma, Pr, Bi). The four critical curves correspond to two thresholds ($G_{thres} = 1$ and $G_{thres} = 100$) and two types of initial pertubation (temperature and velocity). The theoretical critical curves divide the experimental points corresponding to regions of convection or pure conduction in a satisfactory manner. The temperature perturbation critical curve is above the velocity one. This analysis in the thickness/viscosity plane shows again that the bandwidth of uncertainty due to the choice of threshold G_{thres} and perturbation types is not very broad and does not modify the order of magnitude of the critical thickness.

6. Conclusion

This paper presents a novel linear stability analysis of an unsteady base state within the general conceptual framework of amplification theory. The non-normal approach is used, which possesses the advantage over more classical methods to solve the transient problem in a mathematically rigorous way. In turn, this allows one to test other approximations. Here we have applied this approach for the first time to characterize the stability of a transient Rayleigh–Bénard–Marangoni problem in an horizontal fluid layer suddenly cooled from above. It provides the upper limit of the energy amplification that a disturbance of wavenumber k can reach at time t. This quantity reaches a maximum at time $t = t_{opt}(Ma, Ra, Bi, Pr)$, for a specific optimal wavenumber $k_{opt}(Ma, Ra, Bi, Pr)$ and a specific perturbation structure in z. These latter two quantities play the role of the most amplified wavenumber and most amplified mode for the standard steady analysis.

A 'stability' diagram in the space (Bi, Pr, Ma, Ra) has been determined for the pure Marangoni and the pure Rayleigh problem by the non-normal approach. Note that the marginal conditions used to determine the stability curve was obtained by setting the optimal amplification equal to 1 or 100. The critical time and critical wavenumber were evaluated for these marginal conditions. Critical Marangoni and Rayleigh numbers exhibit a strong dependency on the Biot number and a weak sensitivity to Prandtl number variations in the range $Pr \geqslant 1$. Scaling exponents for critical Rayleigh or critical Marangoni versus Biot numbers have been found numerically and confirmed by scaling analysis in the limit of very small and very large Biot numbers. Comparison of the non-normal approach with the frozen-time approximation (a classical quasi-static approach) shows similar results for the critical Marangoni or Rayleigh numbers and the critical wavenumbers. Moreover, the 'blurriness' inherent in any transient problem was analysed as a function of the amplification threshold values and perturbation types. It has been shown that the transition region is thin compared to the large domain of Rayleigh or Marangoni numbers covered by the analysis.

Finally, a comparison with experimental results has been performed, where convection is induced by solvent evaporation during the drying of polymer solution. A good agreement was indeed found between the present theoretical study and experimental observations. The method was developed in this paper for the cooling of a fluid induced by solvent evaporation but could easily be extended to other transient problems.

Supplementary material is available at journals.production.org/FLM.

REFERENCES

ANDERSSON, P., BERGGREN, M. & HENNINGSON, D. S. 1999 Optimal disturbances and bypass transition in boundary layers. *Phys. Fluids* **11**, 134–150.

BERG, J. C., BOUDART, M. & ACRIVOS, A. 1966 Natural convection in pools of evaporating liquids. *J. Fluid Mech.* **24**, 721–735.

BHADAURIA, B. S. & BATHIA, P. K. 2002 Time-periodic heating of Rayleigh–Benard convection. *Phys. Scr.* **66**, 59–65.

BODENSCHATZ, E., PESCH, W. & AHLERS, G. 2000 Recent developments in Rayleigh–Bénard convection. *Annu. Rev. Fluid Mech.* **32**, 709–778.

CHANDRASEKHAR, S. 1961 *Hydrodynamic and Hydromagnetic Stability*. Oxford University Press.

COLINET, P., JOANNES, L., IORIO, C. S., HAUTE, B., BESTEHORN, M., LEBON, G. & LEGROS, J. C. 2003 Interfacial turbulence in evaporating liquids: theory and preliminary results of the itel-master 9 sounding rocket experiment. *Adv. Space Res.* **32** (2), 119–127.

COLINET, P., LEGROS, J. C. & VELARDE, M. G. 2001 *Nonlinear Dynamics of Surface-Tension-Driven Instabilities*. Wiley-VCH.

CURRIE, I. G. 1967 The effect of heating rate on the stability of stationary fluids. *J. Fluid Mech.* **29**, 337–347.

DAVIS, S. H. 1987 Thermocapillary instabilities. *Annu. Rev. Fluid Mech.* **19**, 403–435.

ECKERT, K., ACKER, M. & SHI, Y. 2004 Chemical pattern formation driven by a neutralization reaction. I. Mechanism and basic features. *Phys. Fluids* **16** (2), 385–399.

FARRELL, B. F. & IOANNOU, P. J. 1996 Generalized stability theory. Part I. Autonomous operators. *J. Atmos. Sci.* **53**, 2025–2040.

FOSTER, T. D. 1965 Stability of a homogeneous fluid cooled uniformly from above. *Phys. Fluids* **8**, 1249–1257.

GOUSSIS, D. A. & KELLY, R. E. 1990 On the thermocapillary instabilities in a liquid layer heated from below. *Intl J. Heat Mass Transfer* **33**, 2237–2245.

HOMSY, G. M. 1973 Global stability of time-dependent flows: impulsively heated or cooled fluid layers. *J. Fluid Mech.* **60**, 129–139.

KANG, K. H. & CHOI, C. K. 1997 A theoretical analysis of the onset of surface-tension-driven convection in a horizontal liquid layer cooled suddenly from above. *Phys. Fluids* **9**, 7–15.

LICK, W. 1965 The instability of a fluid layer with time-dependent heating. *J. Fluid Mech.* **21**, 565–576.

LUCHINI, P. 2000 Reynolds-number-independent instability of the boundary layer over a flat surface: optimal perturbations. *J. Fluid Mech.* **404**, 289–309.

MANCINI, H. & MAZA, D. 2004 Pattern formation without heating in an evaporative convection experiment. *Europhys. Lett.* **66**, 812–818.

MERKT, D. & BESTEHORN, M. 2003 Bénard–Marangoni convection in a strongly evaporating fluid. *Physica* D **185**, 196–208.

MOUSSY, C., LEBON, G. & MARGERIT, J. 2004 Influence of evaporation on Bénard–Marangoni instability in a liquid–gas bilayer with a deformable interface. *Eur. Phys. J.* B **40**, 327–335.

NEPOMNYASHCHY, A., SIMANOVSKII, I. & LEGROS, J. C. 2006 *Interfacial Convection in Multilayer Systems*. Springer.

OZEN, O. & NARAYANAN, R. 2004 The physics of evaporative and convective instabilities in bilayer systems: linear theory. *Phys. Fluids* **16**, 4644–4652.

PEARSON, J. R. A. 1958 On convection cells induced by surface tension. *J. Fluid Mech.* **4**, 489–500.

RAPAKA, S., CHEN, S., PAWAR, R. J., STAUFFER, P. H. & ZHANG, D. 2008 Non-modal growth of perturbations in density-driven convection in porous media. *J. Fluid Mech.* **609**, 285–303.

RAYLEIGH, L. 1916 On convection currents in a horizontal layer of fluid when the higher temperature is on the under side. *Phil. Mag.* **32**, 529–546.

REDDY, S. C., SCHMID, P. J., BAGGET, P. & HENNINGSON, D. S. 1998 On the stability of streamwise streaks and transition thresholds in plane channel flow. *J. Fluid Mech.* **365**, 269–303.

REICHENBACH, J. & LINDE, H. 1981 Linear perturbation analysis of surface-tension-driven convection at a plane interface (Marangoni instability). *J. Colloid Interface Sci.* **84**, 433–443.

ROSENBLAT, S. & TANAKA, G. A. 1971 Modulation of thermal convection instability. *Phys. Fluids* **14**, 1319–1322.

SCHATZ, M. F., VANHOOK, S. J., MCCORMICK, W. D., SWIFT, J. B. & SWINNEY, H. L. 1995 Onset of surface-tension-driven Bénard convection. *Phys. Rev. Lett.* **75**, 1938–1941.

SCHMID, P. J. & HENNINGSON, D. S 2001 *Stability and Transition in Shear Flows*. Springer.

SCRIVEN, L. E. & STERNLING, C. V. 1964 On cellular convection driven by surface-tension gradients: effects of mean surface tension and surface viscosity. *J. Fluid Mech.* **19**, 321–340.

SPARROW, E. M., GOLDSTEIN, R. J. & JONSSON, V. K. 1963 Thermal instability in a horizontal fluid layer: effect of boundary conditions and nonlinear temperature profile. *J. Fluid Mech.* **18**, 513–528.

TOUAZI, O., CHÉNIER, E., DOUMENC, F. & GUERRIER, B. 2010 Simulation of transient Rayleigh–Bénard–Marangoni convection induced by evaporation. *Intl J. Heat Mass Transfer*. **53**, 656–664.

TOUSSAINT, G., BODIGUEL, H., DOUMENC, F., GUERRIER, B. & ALLAIN, C. 2008 Experimental characterization of buoyancy- and surface tension-driven convection during the drying of a polymer solution. *Intl J. Heat Mass Transfer* **51**, 4228–4237.

VIDAL, A. & ACRIVOS, A. 1968 Effect of nonlinear temperature profiles on onset of convection driven by surface tension gradients. *Ind. Engng Chem. Fundam.* **7**, 53–58.